

Superheating control of an Organic Rankine Cycle for recovering waste heat from an engine cooling system

Donatien Dubuc, Paolino Tona

▶ **To cite this version:**

Donatien Dubuc, Paolino Tona. Superheating control of an Organic Rankine Cycle for recovering waste heat from an engine cooling system. Control Engineering Practice, 2020, 101, pp.104519. 10.1016/j.conengprac.2020.104519 . hal-02913074

HAL Id: hal-02913074
https://ifp.hal.science/hal-02913074

Submitted on 7 Aug 2020

HAL is a multi-disciplinary open access archive for the deposit and dissemination of scientific research documents, whether they are published or not. The documents may come from teaching and research institutions in France or abroad, or from public or private research centers.

L'archive ouverte pluridisciplinaire **HAL**, est destinée au dépôt et à la diffusion de documents scientifiques de niveau recherche, publiés ou non, émanant des établissements d'enseignement et de recherche français ou étrangers, des laboratoires publics ou privés.

Superheating control of an Organic Rankine Cycle for recovering waste heat from an engine cooling system

Donatien Dubuc[a], Paolino Tona[a]

[a] *Control, Signal and System Department - IFP Energies nouvelles, Rond-point de l'échangeur de Solaize BP3, 69360 Solaize, France*

Abstract

This paper proposes a set of strategies to control the superheat (SH) value of an Organic Rankine Cycle (ORC). This ORC corresponds to an experimental test bench aimed at developing a waste heat recovery system to be connected to the cooling circuit of a light-duty vehicle. Three strategies have been developed and tested experimentally. The first one is a linear control based on a PI controller valid for a given operating point. The second, valid for the same operating point, proposes an LPV (Linear Parameter-Varying) approach, less conservative and more accurate than the first one. Finally, a third strategy also using the LPV framework provides a controller valid in the full operating range of the test bench.

Keywords: Organic Rankine Cycle, LPV systems, H_∞ control, automotive, Waste Heat Recovery.

1. Introduction

The aim of this paper is to propose a control strategy for an Organic Rankine Cycle used to recover the heat dissipated in an engine cooling system. The system, briefly called ORC in the sequel, corresponds to an experimental test bench installed at IFP Energies nouvelles in Lyon (depicted in Figure 1) and aimed at developing an industrial waste heat recovery solution for a light-duty vehicle.

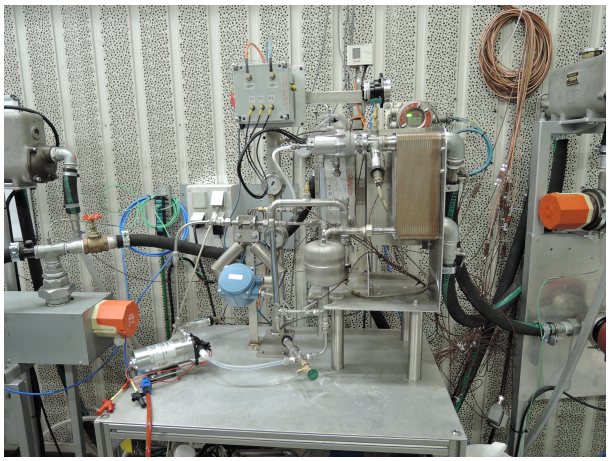


Figure 1: Test bench view at IFP Energies Nouvelles

The ORC is schematically described in Figure 2. The working fluid inside the ORC is a Novec^{TM} 649, a commercial heat transfer fluid. It is moved by a volumetric pump that can be controlled in voltage from 0 to 10 V. The hot source, represented by the red circuit in Figure 2 consists of water heated at a controlled temperature T_{evap} and circulating in the evaporator (or boiler) which permits to transform the working fluid into vapor. The energy thus recovered is converted into mechanical energy by a turbine. The cold source contains water at the controlled temperature T_{cond} which circulates in the condenser and brings the working fluid back to liquid state. The evaporator of the test bench is a plate heat exchanger designed to exchange 18 kW of heat for a hot source at 115 °C.

For more details on the operation and the architectures of ORCs, see for example [1] and [2]. The main ORC applications in the automotive industry since the 1970s are described in [3]. Regarding control strategies, a recent state of the art is presented in [4]. Examples of control strategies specific to the automotive area are described in [5]. It should be noted that, to the best of our knowledge, there is no documented research on the control of ORC systems that recover heat from engine coolant in a road vehicle. These systems are usually considered simpler to design and to deal with than ORCs for waste heat recovery from exhaust gas, but may actually prove challenging to control, depending on the variability of the operating conditions induced by the specificities of the cooling system. Even if the methodologies developed in this paper aim at controlling a low-temperature ORC for automotive applications, they could be easily extended to other Rankine-based waste heat recovery systems.

The key variable to control an ORC is the superheat SH. Superheat is defined as the difference between the fluid temperature and the saturation temperature (at a

Email addresses: donatien.dubuc@ifpen.fr (Donatien Dubuc), paolino.tona@ifpen.fr (Paolino Tona)

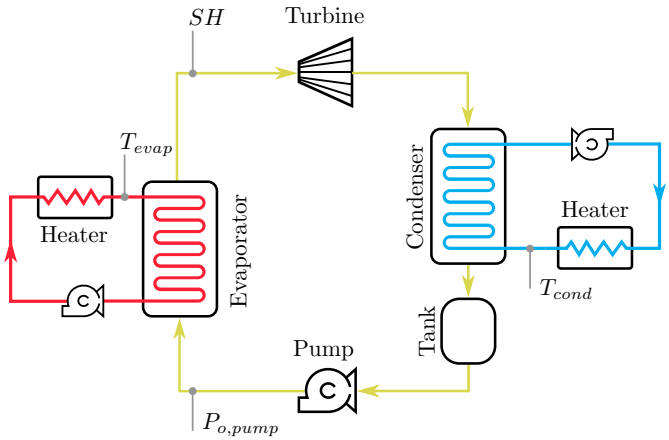


Figure 2: Test bench architecture of the ORC

given pressure) when the fluid changes to the liquid state. In summary:

$$SH = T_{fluid} - T_{sat}(pressure) \tag{1}$$

where, $T_{sat}(pressure)$ is given by known maps.

It is commonly accepted that the lower the superheat, the more energy is absorbed by the working fluid. Therefore, more mechanical energy can be recovered by the expansion machine (here, a kinematic turbine). Besides, the superheat has to be positive to ensure that the Rankine cycle operates properly and does not damage the components. It is the mass flow rate of the working fluid through the evaporator that regulates the superheat. From a practical point of view, for given temperatures T_{evap} and T_{cond}, an increase in this flow rate, and consequently in the pump command voltage, will lead to a decrease in superheat (at steady state).

Remark 1.1. *Note that the water flows in the cold and hot sources are kept constant. Thus, only the variables T_{evap} and T_{cond} define the operating point.*

The objective of this paper is to design, from experimental data, a controller that regulates superheat via the pump voltage as shown in Figure 3. Two cases will be studied:

(1) A local control valid for a given operating point.

(2) A global control valid regardless of the operating point, which is also capable of rejecting temperature disturbances for a fixed reference.

Following the work of [6] and [7], a simple PI controller will be designed based on a linear model identified from experimental data to deal with the first case. This controller, experimentally tested, will be used as a reference to be improved. Then, based on the same experimental data, an LPV model will be identified. From this model,

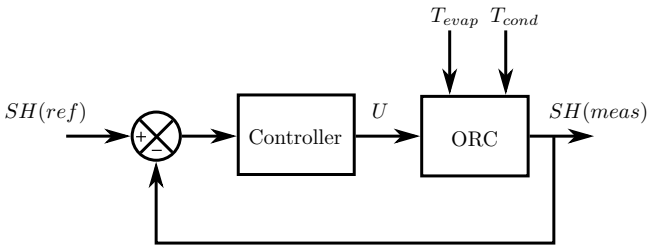


Figure 3: Superheat control scheme

an $\mathcal{H}_\infty$ LPV controller will be designed and validated on the test bench. The second case, more representative of the real operation, significantly increases the complexity of the system. To deal with it, the previous methodology is extended and also experimentally validated.

Among the variables measured or estimated on the test bench, those represented in Figure 2 will be used, depending on the controller to be designed:

(1) The water temperature at the evaporator inlet T_{evap};

(2) The water temperature at the condenser inlet T_{cond};

(3) The pressure at the pump outlet $P_{o,pump}$;

(4) The superheat SH value estimated using a pressure and temperature sensor plus a map provided by the REFPROP thermophysical property database [8].

Finally, it should be noted that all controllers defined in continuous time have been discretized by the Euler method with a sampling time of 0.02 s. Then, they have been included in the embedded software via Simulink Coder and the test bench control software Morphee 2.

2. Contributions

This paper provides the following contributions:

(1) Superheat control design for ORC systems that recover heat from engine coolant.

(2) LPV ORC modeling from experimental data and methodology to obtain these data.

(3) $\mathcal{H}_\infty$ LPV controller design applied to said LPV model.

(4) Experimental validations of the controllers.

3. Control for a given operating point

This section is devoted to solving the problem of tracking several superheat levels for a given ORC operating point. With the architecture of the test bench in Figure 2, this point is defined by the temperature pair (T_{evap}, T_{cond}).

In this part of the study, the temperature references for T_{evap} and T_{cond} are set at 80 °C and 30 °C respectively.

Note that, although these temperatures are controlled by two PID implemented in a programmable logic controller (PLC), they can vary by 1 °C around the references as shown in Figure 4.

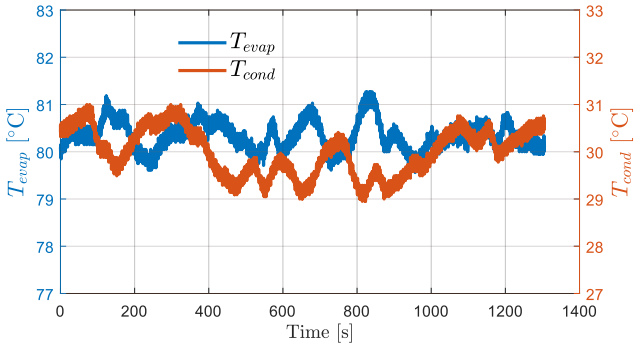


Figure 4: Chosen operating point

3.1. Preliminary analysis and identification protocol

To design a control-oriented model, a black-box approach will be used. The ORC system will be excited via the pump control voltage, then a model describing the dynamics of the superheat will be identified.

In order to get an overview of the ORC behavior, let us submit the system to a train of voltage steps as shown in Figure 5.

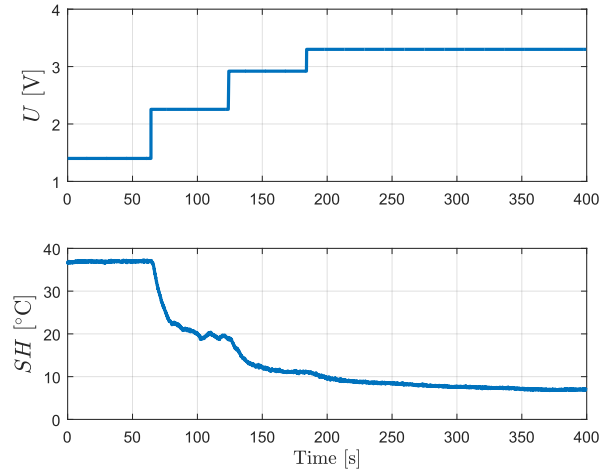


Figure 5: Steps submitted to the ORC

The steady state values can be closely approximated by a linear regression, as shown in Figure 6. Thus, it can be assumed that the static gain of the system follows a linear trend of $-15.7\,°\mathrm{C\,V^{-1}}$. On the other hand, the analysis of the superheat settling time in Figure 5 shows a non-linear behavior. Indeed, steady state is reached in about 40 s for high superheat values and more than 100 s for low ones.

This first basic analysis leads to the conclusion that the ORC is a non-linear system. We therefore need an input

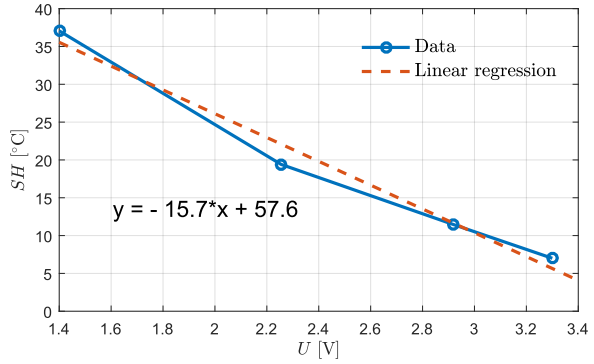


Figure 6: Linear regression of the steady state values

signal which permits to excite the system on several levels of intensity. That is why a multi-level pseudo-random sequence (mPRS) [9] will be used. Unlike the pseudo-random binary sequence (PRBS) which provides two excitation levels, mPRS provides several excitation levels while maintaining an autocorrelation function similar to white noise. It is therefore particularly suitable for non-linear systems.

Following the methodology described in [9], a sequence is generated from the GALOIS[1] software. A 7-level signal with two shift registers has been generated, with a switching time of 25 s and a multiple of 2 harmonic suppression. This results in the voltage command sequence presented in Figure 7, to be applied to the system.

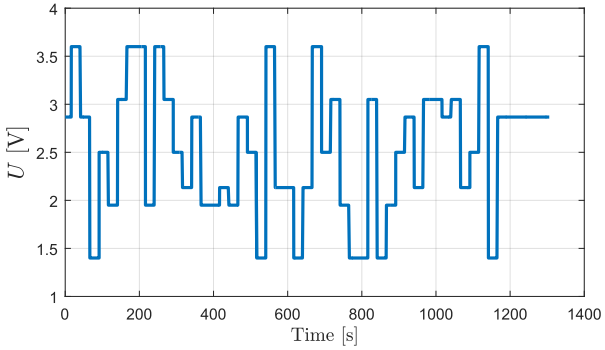


Figure 7: mPRS voltage

3.2. Linear identification and control

3.2.1. First-order system identification

For comparison purposes, let us design a controller that will serve as a reference for the sequel. As mentioned in [6] and [7], it is possible to approximate the system by several first order plus time delay transfer functions, depending

[1]GALOIS can be downloaded at:
`https://warwick.ac.uk/fac/sci/eng/research/grouplist/biomedicaleng/bbsl/signal_design/galois`

on the operating point. As it can be seen in Figure 5, the delay between the command U and superheat SH can be neglected. Thus, for the operating point $(T_{evap}, T_{cond}) = (80\,°C, 30\,°C)$ let us try to approximate the system by:

$$FOTF \triangleq \frac{\Delta SH(s)}{\Delta U(s)} = \frac{K}{\tau s + 1} \tag{2}$$

To identify (2), the mPRS illustrated in Figure 7 is applied to the ORC. The result is the data depicted in Figure 8, where ΔSH represents the output to be identified and ΔU the input. Each signal is sampled at a rate of 0.1 s and consists of 13×10^3 points.

To analyze the performance of the different identified models, we will use the FIT index defined as follows:

Definition 3.1. *Given, an observation vector data x, and its estimate $\hat{x}$, the fit index is defined as:*

$$FIT = 1 - \frac{\|x - \hat{x}\|_2}{\|x - mean(x)\|_2} \tag{3}$$

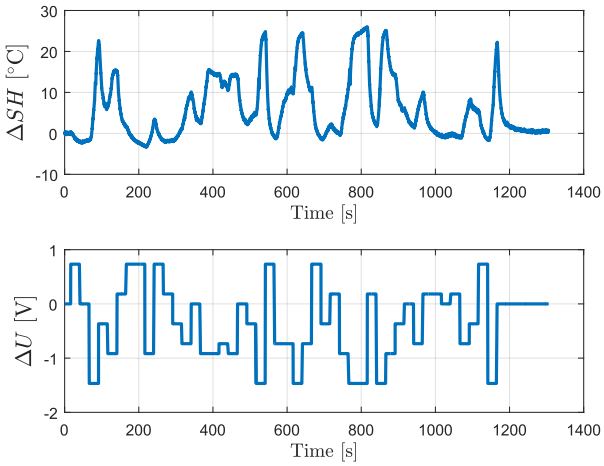


Figure 8: Data used for identification of $FOTF$

Then, the identification through the MATLAB function `tfest` yields the following transfer function:

$$FOTF = \frac{-16.1}{18.07s + 1}, \tag{4}$$

which corresponds to the results obtained in Figure 9. The static gain found is $-16.1\,°C\,V^{-1}$ which is consistent with the one established by the linear regression in Section 3.1.

The obtained performance index FIT is only 63.5% which is explained by the model inability to capture the dynamics at low superheat values. Indeed, as explained in Section 3.1, the time constant becomes significantly large for these values. Thus a fixed time constant cannot model the behavior of this part of the system.

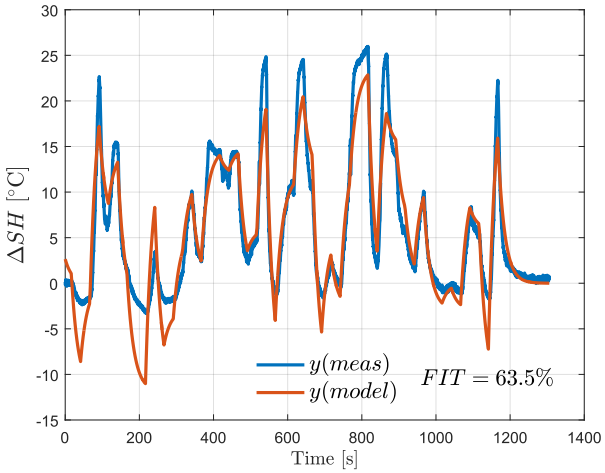


Figure 9: Identification results of $FOTF$

3.2.2. PI controller design

To find the coefficients K_p and K_i of the following PI controller:

$$PI(s) = K_p + \frac{K_i}{s}, \tag{5}$$

the control scheme presented in Figure 10 will be used, where the ORC system will be represented by the transfer function (4).

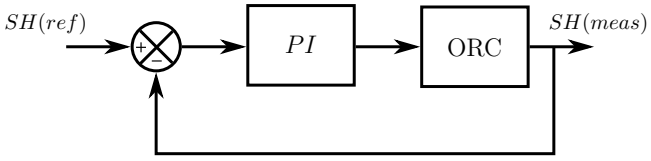


Figure 10: Block diagram of the PI regulation

To obtain a controller robust to model uncertainties, the coefficients K_p and K_i are chosen such that the phase margin is 90° and the closed-loop bandwidth is $0.01\,rad\,s^{-1}$. This gives:

$$K_p = -0.156 \quad \text{and} \quad K_i = -0.00838 \tag{6}$$

3.2.3. Experimental results of the PI controller

By setting the setpoint of T_{evap} and T_{cond} to 80 °C and 30 °C respectively, reference steps are applied to the real system integrating the PI controller (6). The results obtained are presented in Figure 11.

The control performance is good enough for superheat values around 15 °C where steady state is reached in about 20 s without exceeding the set point. However, an overshoot appears for lower superheat values, which becomes larger and larger as the superheat decreases. Besides, the settling time increases to over 100 s then to over 200 s for the last step.

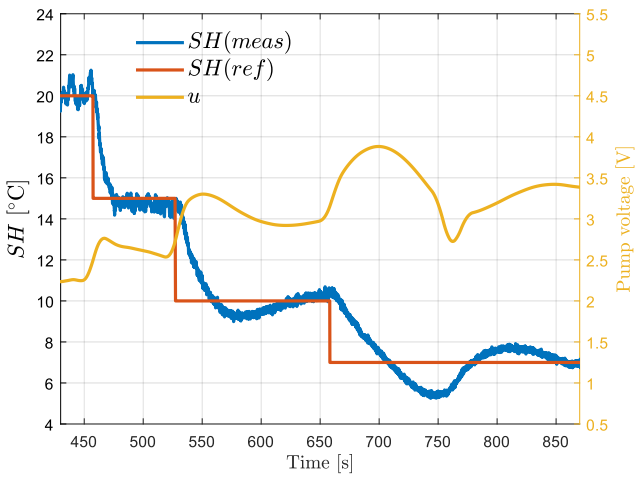


Figure 11: PI control for a given operating point

Nevertheless, the PI controller has proven to be able to control different levels of superheat for a given ORC operating point. More complex PI controllers, with a feedforward loop, for instance, could improve the tracking performance as in [10].

This first simple control strategy will be used as a reference to be improved in the sequel.

3.3. LPV-based regulation

In order to improve the results, in particular those of the ORC modeling, a linear parameter-varying (LPV) approach is considered [11, 12]. The objective here is to obtain, via an experimental system identification, an LPV model and then a controller based on this model. To our knowledge, this kind of global approach has never been studied for ORCs, though related research does exist in the literature. Indeed, in [13], the authors do propose an LPV approach for an air conditioning system, but via the linearization of a non-linear physical model. The work in [14] proposes an LPV formulation for an ORC system which is also based on a physical model, but the validation is carried out only in simulation.

3.3.1. Choice of the LPV model and identification

The structure of the LPV system to be identified is chosen as follows:

$$\begin{aligned} \dot{x} &= A(\rho)x + Bu \\ y &\triangleq SH(model) - y_0 = Cx \end{aligned} \tag{7}$$

with,

$$A(\rho) = \begin{bmatrix} \rho_1 & 1 \\ \rho_2 & 0 \end{bmatrix}, \quad B = \begin{bmatrix} 0 \\ b_0 \end{bmatrix}, \quad \text{and} \quad C = \begin{bmatrix} 1 & 0 \end{bmatrix} \tag{8}$$

where y is the superheat minus a constant bias y_0, u is the pump voltage command, b_0 is a constant and the varying parameters ρ_1 and ρ_2 are defined as:

$$\begin{aligned} \rho_1 &= a_{10} + a_{11}P_{o,pump} + a_{12}P_{o,pump}^2 + a_{13}P_{o,pump}^3 \\ \rho_2 &= a_{20} + a_{21}P_{o,pump} + a_{22}P_{o,pump}^2 + a_{23}P_{o,pump}^3. \end{aligned} \tag{9}$$

The variables ρ_1 and ρ_2 are assumed to be bounded. Thus, we can write that:

$$\begin{aligned} \rho \in \mathcal{P}_\rho := \{\rho = [\rho_1 \quad \rho_2]^T \in \mathbb{R}^2 \\ \text{s.t } \rho_1 \in [\underline{\rho_1},\ \overline{\rho_1}] \text{ and } \rho_2 \in [\underline{\rho_2},\ \overline{\rho_2}]\} \end{aligned} \tag{10}$$

The choice of the external variable $P_{o,pump}$ is motivated by the fact that it is a good image of the physical state of the working fluid. In addition, it corresponds to a realistic sensor choice, since this pressure will most certainly be measured in the industrial application.

The system composed by (7)-(9) has 10 unknown parameters to be identified. There exist several papers dealing with techniques for identifying LPV systems, such as [15] and [16]. However, since (7) is continuous with a bias y_0 to be estimated, the unknown parameters will be identified by solving a nonlinear least squares problem with a Levenberg-Marquardt algorithm. In short, to identify the unknown parameters, we will solve the following optimization problem:

$$\begin{aligned} &\min_{b_0, y_0, a_{ij}, (i,j)\in[\![1,2]\!]\times[\![0,3]\!]} \sum (SH(model) - SH(meas))^2 \\ &\text{subject to} \quad (7)\text{-}(9) \end{aligned} \tag{11}$$

Remark 3.1. *From a practical point of view, the system* (7)-(9) *is designed with* Simulink *and the parameters are initialized as follows:* $a_{i,j} = -1$*, to ensure that the model is stable and* $y_0 = 30$*. Then the parameters are optimized with* `lsqnonlin` *command.*

From the same data used to identify the first-order model in Section 3.2 (without the offset) and those representing the pressure in Figure 12, we obtain the results presented at the bottom of Figure 12. The FIT index has increased from 63.5% to 90.0%. All the superheat variations are well modeled, except for the behavior at very low superheat values which is less satisfactorily captured, as can be seen around 200 s in the graph of Figure 12.

The results of a validation test are shown in Figure 13. The model remains very accurate even when applied to data that were not used for identification. Thus, the model is validated for the design of an LPV controller.

3.3.2. Design of an $\mathcal{H}_\infty$ LPV controller

As introduced in [17], if the parameter dependence of an LPV system is affine and bounded, the system can be transformed into a polytopic form which is a convex interpolation of a finite set of linear systems. In our case, since

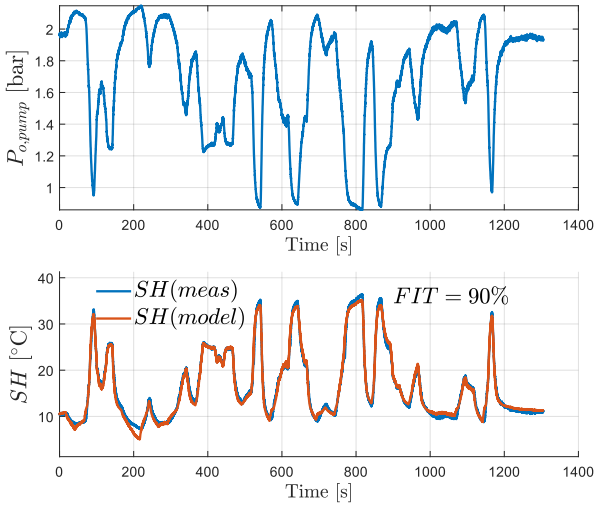


Figure 12: Top: pressure data used to compute ρ_1 and ρ_2. Bottom: LPV identification results for a given operating point

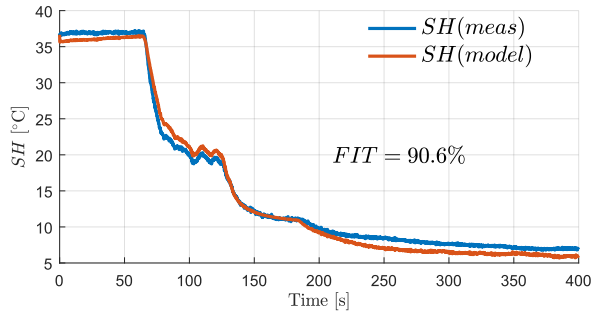


Figure 13: Validation test of the LPV model

the dependence on the parameter vector $\rho \in \mathcal{P}_\rho$ is affine, (7) can be written as:

$$G(\rho): \begin{cases} \dot{x} = \sum_{i=1}^{4} \mu_i(\rho)\,(A_i x) + Bu \\ y = Cx \end{cases} \tag{12}$$

where A_i corresponds to $A(\rho)$ calculated at each vertex of the polytope:

$$A_1 = \begin{bmatrix} \underline{\rho_1} & 1 \\ \underline{\rho_2} & 0 \end{bmatrix}, \quad A_2 = \begin{bmatrix} \overline{\rho_1} & 1 \\ \underline{\rho_2} & 0 \end{bmatrix}$$
$$A_3 = \begin{bmatrix} \underline{\rho_1} & 1 \\ \overline{\rho_2} & 0 \end{bmatrix}, \quad A_4 = \begin{bmatrix} \overline{\rho_1} & 1 \\ \overline{\rho_2} & 0 \end{bmatrix} \tag{13}$$

and μ_i the interpolation functions:

$$\begin{aligned} \mu_1(\rho) &= \left(\frac{\overline{\rho_1} - \rho_1}{\overline{\rho_1} - \underline{\rho_1}}\right) \times \left(\frac{\overline{\rho_2} - \rho_2}{\overline{\rho_2} - \underline{\rho_2}}\right) \\ \mu_2(\rho) &= \left(\frac{\overline{\rho_1} - \rho_1}{\overline{\rho_1} - \underline{\rho_1}}\right) \times \left(\frac{\rho_2 - \underline{\rho_2}}{\overline{\rho_2} - \underline{\rho_2}}\right) \\ \mu_3(\rho) &= \left(\frac{\rho_1 - \underline{\rho_1}}{\overline{\rho_1} - \underline{\rho_1}}\right) \times \left(\frac{\overline{\rho_2} - \rho_2}{\overline{\rho_2} - \underline{\rho_2}}\right) \\ \mu_4(\rho) &= \left(\frac{\rho_1 - \underline{\rho_1}}{\overline{\rho_1} - \underline{\rho_1}}\right) \times \left(\frac{\rho_2 - \underline{\rho_2}}{\overline{\rho_2} - \underline{\rho_2}}\right) \end{aligned} \tag{14}$$

which leads to $\sum_{i=1}^{4} \mu_i(\rho) = 1$.

To obtain a $\mathcal{H}_\infty$ LPV polytopic controller, we will use the block diagram given in Figure 14 where $K(\rho)$ is defined as:

$$K(\rho): \begin{cases} \dot{x}_k = \sum_{i=1}^{4} \mu_i(\rho)\,(A_{ki}x_k + B_{ki}(r-y)) \\ u = \sum_{i=1}^{4} \mu_i(\rho)\,(C_{ki}x_k + D_{ki}(r-y)) \end{cases} \tag{15}$$

where x_k is the internal state of the controller.

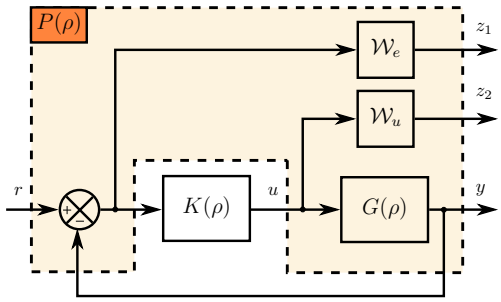


Figure 14: Block diagram to design a $\mathcal{H}_\infty$ LPV polytopic controller

From Figure 14, we can deduce the $\mathcal{H}_\infty$ standard problem depicted in Figure 15. $P(\rho)$ is deduced from the block diagram as:

$$P(\rho): \begin{cases} \dot{x}_e = \sum_{i=1}^{4} \mu_i(\rho)\,(A_{ei}x_e + B_{1i}r) + B_2 u \\ z = \sum_{i=1}^{4} \mu_i(\rho)\,(C_{1i}x_e + D_{11i}r) + D_{12}u \\ r - y = C_2 x_e + D_{21} r \end{cases} \tag{16}$$

where x_e is the extended state determined from the block diagram.

To solve this standard problem, we need to find the matrices A_{ki}, B_{ki}, C_{ki}, D_{ki}, $i = 1, \ldots, 4$ of (15) such that:

(1) The closed loop in Figure 15 is stable;

(2) The upper bound γ of the induced-$\mathcal{L}_2$ norm from the reference r to z is minimized, *i.e*:

$$\min \gamma \quad \text{s.t} \quad \sup_{r \neq 0, r \in \mathcal{L}_2} \frac{\|z\|_2}{\|r\|_2} \leq \gamma \tag{17}$$

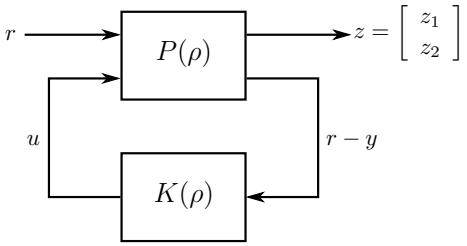


Figure 15: Standard formulation

To fulfill these conditions, the following proposition will be used:

Proposition 3.1 ([18]). *Consider the LPV polytopic controller* (15) *and the LPV polytopic system* (12)*. The standard problem is solved, if there exist matrices* Y, X *and* $\tilde{A}_i$, $\tilde{B}_i$, $\tilde{C}_i$, $\tilde{D}_i$, $i = 1, \ldots, 4$ *such that the following LMIs hold for all* $i = 1, \ldots, 4$*:*

$$\begin{aligned} &\min \ \gamma \\ &s.t \begin{bmatrix} M_{11} & * & * & * \\ M_{21} & M_{22} & * & * \\ M_{31} & M_{32} & M_{33} & * \\ M_{41} & M_{42} & M_{43} & M_{44} \end{bmatrix} \prec 0 \\ &\begin{bmatrix} X & I_{n_x} \\ I_{n_x} & Y \end{bmatrix} \succ 0 \end{aligned} \tag{18}$$

where,

$$\begin{aligned} M_{11} &= A_{ei}X + XA_{ei}^T + B_{2i}\tilde{C}_i + \tilde{C}_i^T B_{2i}^T \\ M_{21} &= \tilde{A}_i + \left(A_{ei} + B_{2i}\tilde{D}_i C_{2i}\right)^T \\ M_{22} &= YA_{ei} + A_{ei}^T Y + \tilde{B}_i C_{2i} + \left(\tilde{B}_i C_{2i}\right)^T \\ M_{31} &= \left(B_{1i} + B_{2i}\tilde{D}_i D_{21i}\right)^T \\ M_{32} &= \left(YB_{1i} + \tilde{B}_i D21i\right)^T \\ M_{33} &= -\gamma I_{n_w} \\ M_{41} &= C_{1i}X + D_{12i}\tilde{C}_i \\ M_{42} &= C_{1i} + D_{12i}\tilde{D}_i C_{2i} \\ M_{43} &= D_{11i} + D_{12i}\tilde{D}_i D_{21i} \\ M_{44} &= -\gamma I_{n_z} \end{aligned} \tag{19}$$

The reconstruction of the filter $K(\rho)$ *is obtained by the following equivalent transformation,*

$$\begin{cases} D_{fi} = \tilde{D}_i \\ C_{fi} = \left(\tilde{C}_i - \tilde{D}_i C_{2i} X\right)\left(M^T\right)^{-1} \\ B_{fi} = N^{-1}\left(\tilde{B}_i - YB_{2i}\tilde{D}_i\right) \\ A_{fi} = N^{-1}(\tilde{A}_i - YA_{ei}X - YB_{2i}\tilde{D}_i C_{2i}X - \\ \qquad N\tilde{B}_i C_{2i}X - YB_{2i}\tilde{C}_i M^T)\left(M^T\right)^{-1} \end{cases} \tag{20}$$

where M *and* N *are defined such that* $MN^T = I_{n_x} - XY$ *which can be solved through a singular value decomposition plus a Cholesky factorization.*

Let us denote the sensitivity functions, $S_{r,e}$ the transfer from the reference r to $e = r - y$; and $S_{r,u}$ the transfer from r to the command u. Since Proposition 3.1 minimizes the induced-$\mathcal{L}_2$ norm from r to z by γ, it is clear that (with a slight abuse of language since the system considered is LPV):

$$\sup_{r\neq 0, r\in\mathcal{L}_2} \frac{\|z\|_2}{\|r\|_2} \leq \gamma \quad \Rightarrow \quad \begin{cases} \|S_{r,e}\|_\infty \leq \dfrac{\gamma}{\|\mathcal{W}_e\|_\infty} \\ \|S_{r,u}\|_\infty \leq \dfrac{\gamma}{\|\mathcal{W}_u\|_\infty} \end{cases} \tag{21}$$

Thus $\mathcal{W}_e$ and $\mathcal{W}_u$ will shape these two sensitivity functions. Both functions are chosen as first-order filters:

$$\begin{aligned} \mathcal{W}_e^{-1}(s) &= \frac{s + \omega_e \epsilon_e}{\dfrac{s}{M_e} + \omega_e} \\ \mathcal{W}_u^{-1}(s) &= \frac{\epsilon_u s + \omega_u}{s + \dfrac{\omega_u}{M_u}} \end{aligned} \tag{22}$$

To choose the parameters, the following criteria will be used:

(1) The static error must be small with a reduced overshoot and a good robustness. It means that the singular values of $S_{r,e}$ have to be small at low frequencies, without high resonance peak and below $6dB$ (a standard value for a robustness margin).

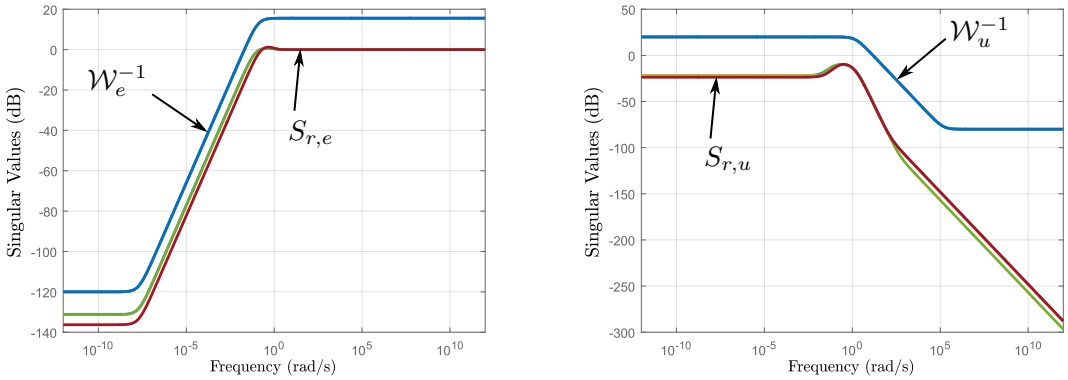
(2) The actuator load must be reduced. It means that the singular values of $S_{r,u}$ have to be small at high frequencies with a reasonable bandwidth.

This leads to the values given in Table 1.

Table 1: Parameter values of the weighting functions

$\mathcal{W}_e^{-1}$		$\mathcal{W}_u^{-1}$	
Parameter	**Value**	**Parameter**	**Value**
ω_e	0.02	ω_u	15
ϵ_e	10^{-6}	ϵ_u	10^{-4}
M_e	6	M_u	10

Applying Proposition 3.1, the controller matrices in Appendix A and the sensitivity functions presented in Figure 16 are obtained. It can be seen that the functions at each vertex of the polytope are "below" the weighting functions. This ensures a small static error without overshoot, good robustness and reduced actuator load.



(a) $S_{r,e}$ (b) $S_{r,u}$

Figure 16: Sensitivity functions at each vertex of the polytope

3.3.3. Experimental results of the $\mathcal{H}_\infty$ LPV controller

By setting the setpoint of T_{evap} and T_{cond} to 80 °C and 30 °C respectively, reference steps are applied to the real system integrating the $\mathcal{H}_\infty$ LPV controller (15). The results obtained are presented in Figure 17.

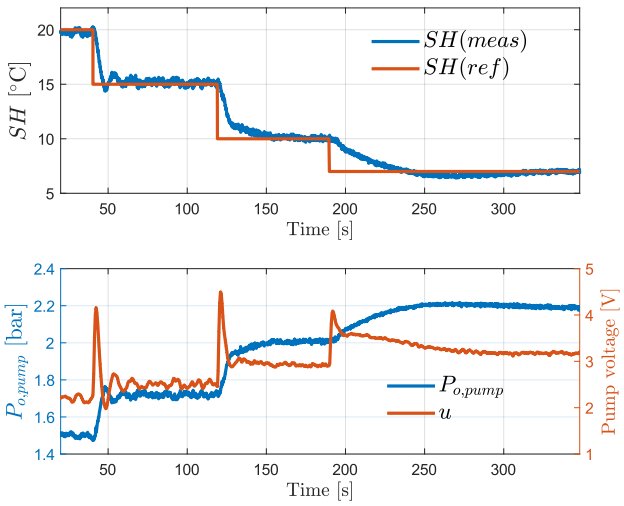


Figure 17: Regulation by the $\mathcal{H}_\infty$ LPV controller for a given operating point

The control performance is very good for superheat values between 20 and 10 °C. Steady-state is reached in about 10 s then 30 s without overshoot. Therefore the performance has been improved compared to the PI controller in Figure 11, mainly because there is no more overshoot for the second step. The quality of the regulation deteriorates for superheat values around 7 °C. Indeed, the steady-state is reached in 120 s with an overshoot of 0.5 °C.

The use of an LPV framework allows to obtain a better representation of the real system. Therefore a more accurate control is possible compared to the linear one. The robustness criteria could be relaxed to improve controller performance.

4. Global control

Unlike the previous section, which focused on controlling different superheat levels for a given operating point (T_{evap}, T_{cond}), this section focuses on controlling superheat regardless of the operating conditions of the ORC.

First, a global test reaching several operating points will be performed. Then, based on the data of this test, we will look for an LPV model describing the evolution of the superheat. The varying parameters will be functions of the pump command, the pressure at the pump outlet and the two water inlet temperatures in the evaporator and condenser. Finally, following the methodology proposed in Section 3.3.2, an $\mathcal{H}_\infty$ LPV controller will be designed and tested on the experimental bench.

4.1. Global identification of an LPV system

In order to perform a global test for the identification, we chose to apply a series of voltage steps for nine different operating points. The test is summarized in Figure 18 with the obtained superheat and the pump voltage. As before, each signal is sampled at a rate of 0.1 s and now consists of 56×10^3 points. Note that the temperatures T_{cond} and T_{evap}, i.e the operating points, are not completely stationary. Indeed, as previously mentioned, the control of T_{cond} and T_{evap} is not very efficient on the test bench.

To identify a model with the data from Figure 18, we choose the same LPV structure as the one defined in (7) and (8) *i.e*:

$$\begin{aligned} \dot{x} &= A(\rho)x + Bu \\ y &\triangleq SH(model) - y_0 = Cx \end{aligned} \tag{23}$$

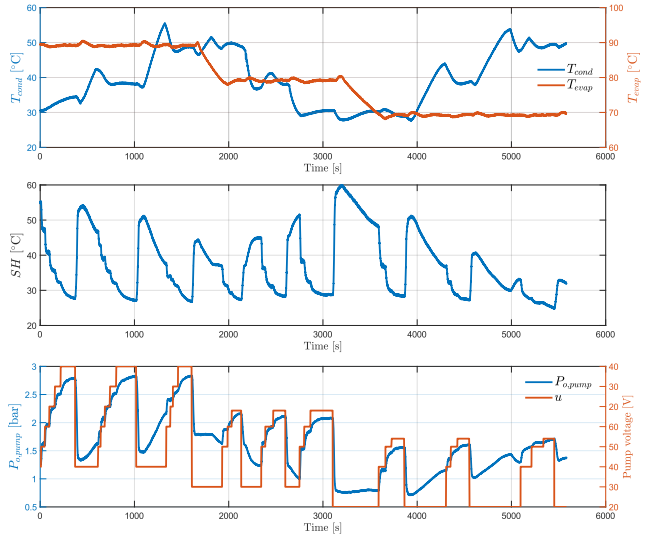


Figure 18: Description of the test used for identification

with,

$$A(\rho) = \begin{bmatrix} \rho_1 & 1 \\ \rho_2 & 0 \end{bmatrix}, \quad B = \begin{bmatrix} 0 \\ b_0 \end{bmatrix} \qquad (24)$$
$$C = \begin{bmatrix} 1 & 0 \end{bmatrix}.$$

But ρ_1 and ρ_2 are now depending on $P_{o,pump}$, T_{evap} and T_{cond}. They have the structure of a multivariate polynomial as below:

$$\begin{aligned}\rho_i =& a_{i0} + a_{i1}P_{o,pump} + a_{i2}P_{o,pump}^2 + a_{i3}P_{o,pump}^3 + \\ & a_{i4}T_{evap} + a_{i5}T_{evap}^2 + a_{i6}T_{evap}^3 + \\ & a_{i7}T_{cond} + a_{i8}T_{cond}^2 + a_{i9}T_{cond}^3 + \\ & a_{i10}P_{o,pump}T_{evap} + a_{i11}P_{o,pump}T_{evap}^2 + \\ & a_{i12}P_{o,pump}^2T_{evap} + a_{i13}P_{o,pump}^2T_{evap}^2 + \\ & a_{i14}P_{o,pump}T_{cond} + a_{i15}P_{o,pump}T_{cond}^2 + \\ & a_{i16}P_{o,pump}^2T_{cond} + a_{i17}P_{o,pump}^2T_{cond}^2 + \\ & a_{i18}T_{evap}T_{cond} + a_{i19}T_{evap}T_{cond}^2 + \\ & a_{i20}T_{evap}^2T_{cond} + a_{i21}T_{evap}^2T_{cond}^2 + \\ & a_{i22}P_{o,pump}T_{evap}T_{cond} + a_{i23}P_{o,pump}T_{evap}T_{cond}^2 + \\ & a_{i24}P_{o,pump}T_{evap}^2T_{cond} + a_{i25}P_{o,pump}T_{evap}^2T_{cond}^2 + \\ & a_{i26}P_{o,pump}^2T_{evap}T_{cond} + a_{i27}P_{o,pump}^2T_{evap}T_{cond}^2 + \\ & a_{i28}P_{o,pump}^2T_{evap}^2T_{cond} + a_{i29}P_{o,pump}^2T_{evap}^2T_{cond}^2 \\ i = (1,2)\end{aligned} \qquad (25)$$

This represents a total of 62 unknown parameters to be identified. As before, we propose to solve the following optimization problem to estimate them:

$$\begin{aligned}&\min_{b_0,y_0,a_{ij},(i,j)\in[\![1,2]\!]\times[\![0,29]\!]} \sum \left(SH(model) - SH(meas)\right)^2 \\ &\text{subject to} \quad (23)\text{-}(25)\end{aligned} \qquad (26)$$

At the end of the optimization, the results presented in Figure 19 are obtained. The FIT performance index is 80.7%, which indicates that the model captures most of the ORC behavior. We can observe that the model is less accurate at the end of the test, where T_{evap} is low and T_{cond} high. At this operating point, heat exchanges and phase changes are not very efficient which may explain the difficulties in modeling this part.

4.2. Synthesis of a global $\mathcal{H}_\infty$ LPV controller

In this section, we will use the notations and structures defined in Section 3.3.2. The system described by (23)-(25) can be written in the polytopic form (12)-(14). The $K(\rho)$ controller is still described by (15).

Unlike the control designed in Section 3.3.2, the main objective of the controller considered here is to reject disturbances represented by temperature variations in the evaporator and condenser. If (23) and (25) are analyzed, these temperature disturbances are not additive but will influence the dynamics of the ORC system in a non-linear way. The goals are: to be robust during the reference change but also to reject these parametric disturbances as quickly as possible. To design an $\mathcal{H}_\infty$ LPV controller, we propose the control scheme described in Figure 20. From this, the same standard problem sketched in Figure 15 can be deduced, where $P(\rho)$ is obtained from Figure 20.

The weighting functions $\mathcal{W}_e$ and $\mathcal{W}_u$ will be defined by (22) and the filter on the reference by:

$$\mathcal{W}_r(s) = \frac{1}{\tau_r s + 1} \qquad (27)$$

To illustrate the capacity of the control scheme in Figure 20 to reject parametric disturbances the control strategy will be first tested on the model (23)-(25). To do this, $K(\rho)$ is designed with Proposition 3.1, using the parameter values in table 2. Then, the following protocol is used: the superheat reference goes from 15 to 10 °C at 250 s; then a fault is simulated at 600 s by changing the values of ρ_1 and ρ_2. The controller design and tests are carried out for $\tau_r = 0$, 10 and 30. The results obtained are presented in Figure 21. We can observe the desired behavior: τ_r adjusts the reference tracking, without impacting the parametric disturbance rejection performance specified by $\mathcal{W}_e$. The final configuration given by Table 2, with $\tau_r = 10$, will be retained. The controller matrices obtained with Proposition 3.1 are presented in Appendix B.

4.3. Experimental results of the global controller

First, the global $\mathcal{H}_\infty$ LPV controller is tested for T_{evap} and T_{cond} references set to respectively 90 °C and 50 °C. Reference steps on the superheat $SH(ref)$ are then applied on the test bench. The results obtained for this operating point are presented in Figure 22. We observe that the system approximately settles in respectively 40 s,

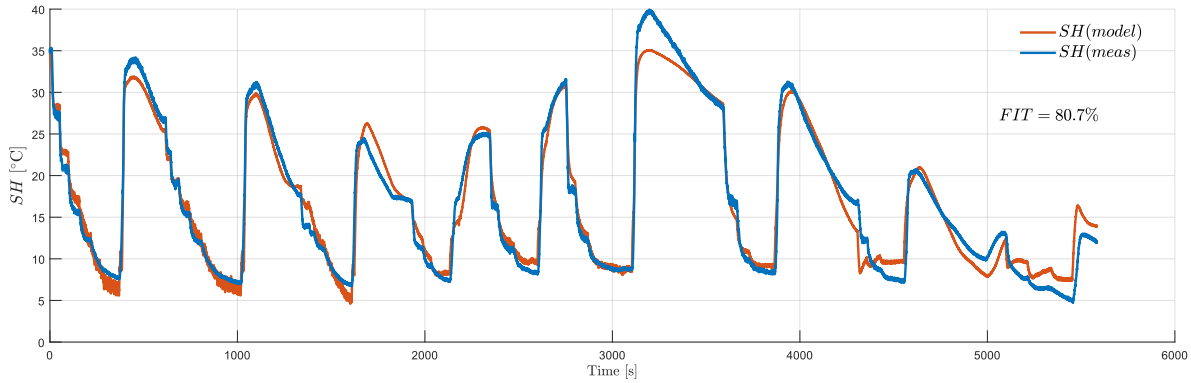


Figure 19: LPV identification results

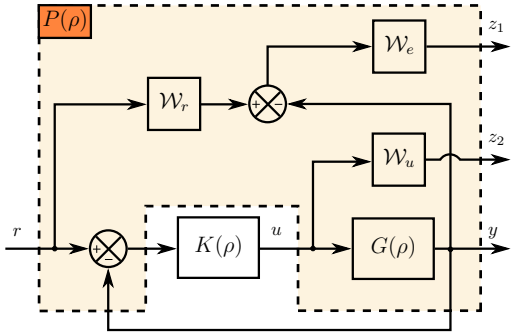


Figure 20: Bloc diagram for a global $\mathcal{H}_\infty$ LPV controller

Table 2: Parameter values of the weighting functions for the global controller

$\mathcal{W}_e^{-1}$		$\mathcal{W}_u^{-1}$	
Parameter	**Value**	**Parameter**	**Value**
ω_e	0.1	ω_u	1
ϵ_e	10^{-6}	ϵ_u	10^{-4}
M_e	6	M_u	10

25 s and then in 15 s with an overshoot close to zero. This matches the simulations carried out in the previous section and meets the desired performance criteria. It can also be seen that the control input variance due to output noise can be large for low superheat values which can lead to a high load on the actuator. Indeed, the variance for u is 0.4 for the PI controller (Figure 11), 0.43 for the first LPV controller (Figure 17) and 0.69 for this one. This point can be improved in a future design.

In order to assess the disturbance rejection performance, $SH(ref)$ is set to 10 °C, then the reference on T_{evap} is changed from 90 to 80 °C. The results depicted in Figure 23 are obtained. During the transient phase the overshoot in superheat reaches a maximum of 0.7 °C and quickly goes back to the reference when T_{evap} stabilizes.

The results are better for T_{cond} variations as it can be seen in Figure 24. Indeed, from Figure 18, one can see that T_{cond} has less influence on the superheat behavior than T_{evap}.

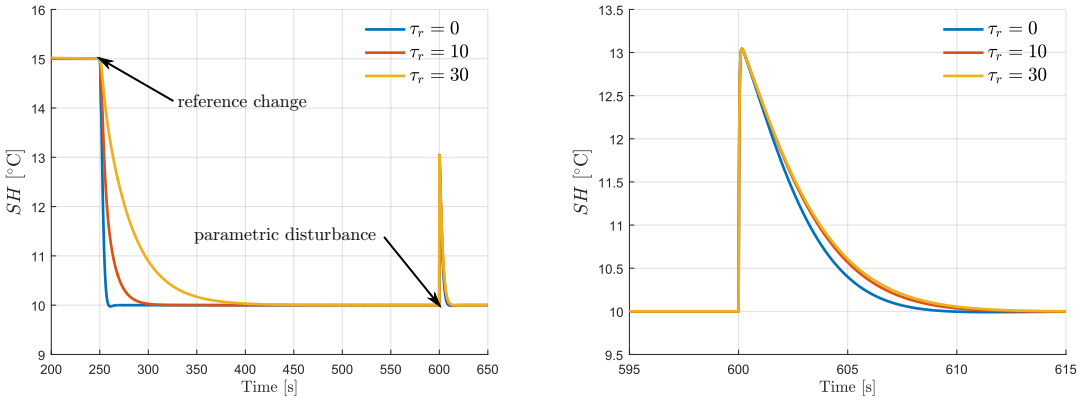
5. Conclusion and further work

In this paper, three different controllers have been designed for the superheat of an ORC system for waste heat recovery from the engine coolant of a light-duty vehicle. First, we have seen that a PI controller can fulfill this role locally, for a given operating point. The design has been based on an identified first-order model and the parameters chosen to obtain a large robustness margin.

Then, to model the superheat as well as possible, an LPV model has been proposed, where the varying parameters depend on the pressure at the pump outlet. It has been established that this model represents the behavior of the system very accurately. Based on this model, an $\mathcal{H}_\infty$ LPV controller has been designed by loop shaping. The control performance has been significantly improved for a given operating point.

Finally, the entire system operation was taken into account in the modeling and the design of a controller. In this case, the varying parameters depend on the pump outlet pressure but also on the temperature of the water in the evaporator and the condenser. The controller has been designed with the objective of rejecting parametric disturbances. Experimental tests have shown the effectiveness of the method for controlling different superheat levels and rejecting the disturbances caused by water temperature changes, in both the hot and cold sources.

Future work will focus on extending the LPV approach to a test bench setup closer to the industrial application. Water flows through the hot and cold sources will be manipulated in order to reproduce operating conditions close to those imposed by the real cooling system during a vehicle standard cycle. Therefore, we will be looking for a model valid for variable mass flows, and a controller based



(a) Whole test

(b) Zoom on disturbance rejection

Figure 21: Control performance for parametric disturbance in simulation

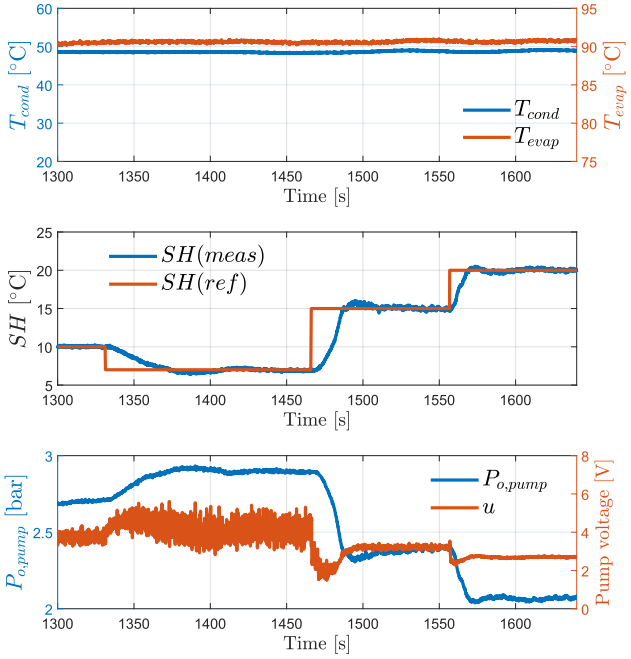


Figure 22: Experimental results of the global $\mathcal{H}_\infty$ LPV controller for a fixed operating point

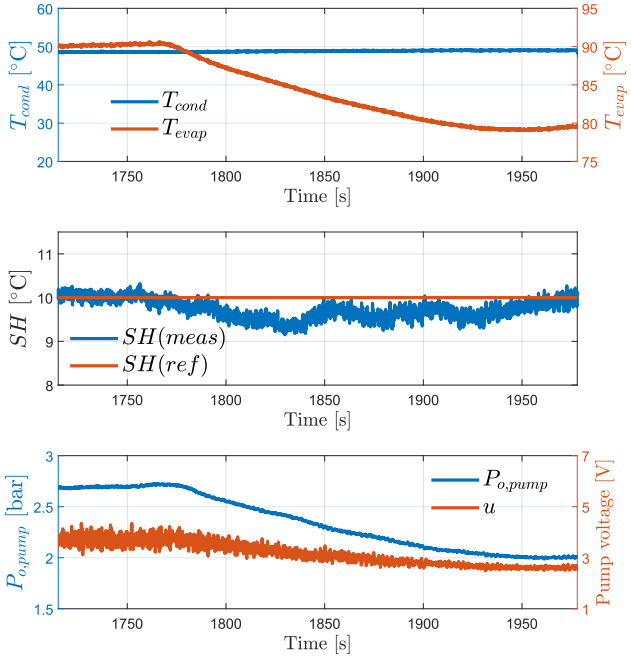


Figure 23: Disturbance rejection of T_{evap}

on this model in order to provide efficient superheat control for the ORC integrated in the vehicle.

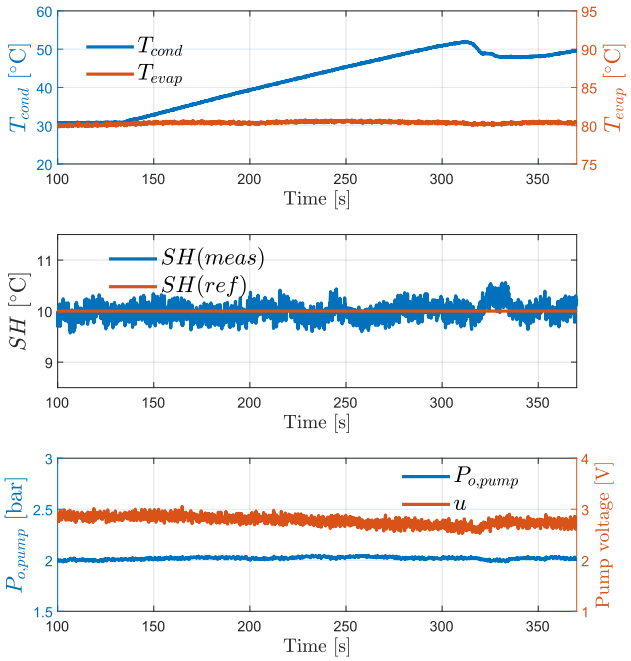


Figure 24: Disturbance rejection of T_{cond}

Appendix A. LPV controller for a given operating point

$$A_{k1} = \begin{bmatrix} -156.6 & -3.3456 & -0.00019167 & 8093.4 \\ 3.763 & 0.062312 & 0.0087353 & -3.6295e+05 \\ 1.9305e-06 & 4.1193e-08 & -1.9828e-08 & -0.0010861 \\ 5.35e-05 & 1.347e-05 & -0.0038333 & -3.5898 \end{bmatrix}$$

$$A_{k2} = \begin{bmatrix} -86.135 & -1.7742 & -0.00019213 & 8093.4 \\ -6.961 & -0.17682 & 0.0087304 & -3.6295e+05 \\ 1.0373e-06 & 2.1275e-08 & -1.9863e-08 & -0.0010861 \\ 4.5712e-05 & 1.3298e-05 & -0.0038354 & -3.5901 \end{bmatrix}$$

$$A_{k3} = \begin{bmatrix} -156.68 & -3.3474 & -0.00019288 & 8093.4 \\ 7.3351 & 0.14196 & 0.0087351 & -3.6295e+05 \\ 1.9412e-06 & 4.1431e-08 & -1.9824e-08 & -0.0010861 \\ 5.3387e-05 & 1.3467e-05 & -0.0038332 & -3.5898 \end{bmatrix}$$

$$A_{k4} = \begin{bmatrix} -86.215 & -1.776 & -0.00019292 & 8093.4 \\ -3.389 & -0.097172 & 0.0087301 & -3.6295e+05 \\ 1.0479e-06 & 2.1513e-08 & -1.9865e-08 & -0.0010861 \\ 4.6314e-05 & 1.3312e-05 & -0.0038356 & -3.5902 \end{bmatrix}$$

$$B_{k1} = \begin{bmatrix} 781.3 \\ -36.753 \\ -1.1828e+08 \\ 144.1 \end{bmatrix} \quad B_{k2} = \begin{bmatrix} 483.65 \\ 43.498 \\ -1.1828e+08 \\ -517.99 \end{bmatrix}$$

$$B_{k3} = \begin{bmatrix} 527.87 \\ -40.002 \\ -1.1828e+08 \\ 148.67 \end{bmatrix} \quad B_{k4} = \begin{bmatrix} 323.41 \\ 50.054 \\ -1.1828e+08 \\ -566.89 \end{bmatrix}$$

$$C_{k1} = \begin{bmatrix} -7.7196e-13 & -9.0051e-15 & 1.0263e-13 & -4.264e-06 \end{bmatrix}$$

$$C_{k2} = \begin{bmatrix} -7.7198e-13 & -9.0053e-15 & 1.0256e-13 & -4.264e-06 \end{bmatrix}$$

$$C_{k3} = \begin{bmatrix} -7.7196e-13 & -9.0051e-15 & 1.0262e-13 & -4.264e-06 \end{bmatrix}$$

$$C_{k4} = \begin{bmatrix} -7.7199e-13 & -9.0055e-15 & 1.0256e-13 & -4.264e-06 \end{bmatrix}$$

$$D_{k1} = D_{k2} = D_{k3} = D_{k4} = 0$$

Appendix B. LPV controller for global control

$$A_{k1} = \begin{bmatrix} -0.83581 & -2.3748 & -0.047259 & 0.11516 & -0.01446 \\ -9.2232 & -60.843 & -0.85356 & -0.14814 & 3.9269e-05 \\ -0.050041 & -3.5088 & -0.079793 & -0.020812 & 0.0035331 \\ -1.8002 & -18.292 & -0.1311 & -0.53102 & 0.061845 \\ -1.2873 & -89.793 & -0.18188 & -2.2034 & -3837.5 \end{bmatrix}$$

$$A_{k2} = \begin{bmatrix} -0.70445 & 0.39243 & -0.029409 & 0.12507 & -0.014443 \\ -7.1229 & -16.602 & -0.56819 & 0.010236 & 0.00039722 \\ -0.042044 & -3.3404 & -0.078706 & -0.020209 & 0.0035411 \\ -1.1328 & -4.2322 & -0.040409 & -0.48069 & 0.061965 \\ 1.2596 & -36.134 & 0.16416 & -2.0113 & -3837 \end{bmatrix}$$

$$A_{k3} = \begin{bmatrix} -0.8853 & -3.4172 & -0.053983 & 0.11143 & -0.014446 \\ -9.2215 & -60.809 & -0.85334 & -0.14802 & 0.00044062 \\ -0.038098 & -3.2572 & -0.07817 & -0.019911 & 0.003542 \\ -1.6153 & -14.395 & -0.10596 & -0.51708 & 0.062002 \\ 0.7223 & -47.459 & 0.091174 & -2.0519 & -3837.4 \end{bmatrix}$$

$$A_{k4} = \begin{bmatrix} -0.75393 & -0.65 & -0.036133 & 0.12134 & -0.014447 \\ -7.1213 & -16.568 & -0.56797 & 0.010357 & 0.00039879 \\ -0.030101 & -3.0888 & -0.077083 & -0.019308 & 0.0035231 \\ -0.94781 & -0.33567 & -0.015274 & -0.46674 & 0.062021 \\ 3.27 & 6.2005 & 0.43733 & -1.8596 & -3837.7 \end{bmatrix}$$

$$B_{k1} = \begin{bmatrix} -100.78 \\ -8.382 \\ 1533 \\ 916.62 \\ 6863.7 \end{bmatrix} \quad B_{k2} = \begin{bmatrix} -100.78 \\ -8.3844 \\ 1533 \\ 916.62 \\ 6864 \end{bmatrix}$$

$$B_{k3} = \begin{bmatrix} -100.78 \\ -8.3842 \\ 1533 \\ 916.62 \\ 6864 \end{bmatrix} \quad B_{k4} = \begin{bmatrix} -100.78 \\ -8.3843 \\ 1533 \\ 916.62 \\ 6863.9 \end{bmatrix}$$

$$C_{k1} = \begin{bmatrix} 0.00036475 & -5.2472e-06 & 9.5986e-06 & -0.00013791 & 1.6418e-05 \end{bmatrix}$$

$$C_{k2} = \begin{bmatrix} 0.00036475 & -5.2472e-06 & 9.5986e-06 & -0.00013791 & 1.6421e-05 \end{bmatrix}$$

$$C_{k3} = \begin{bmatrix} 0.00036475 & -5.2472e-06 & 9.5986e-06 & -0.00013791 & 1.6419e-05 \end{bmatrix}$$

$$C_{k4} = \begin{bmatrix} 0.00036475 & -5.2472e-06 & 9.5986e-06 & -0.00013791 & 1.6417e-05 \end{bmatrix}$$

$$D_{k1} = D_{k2} = D_{k3} = D_{k4} = 0$$

References

[1] S. Quoilin, V. Lemort, The organic Rankine cycle: thermodynamics, applications and optimization, Exergy, Energy system analysis, and Optimization (2011).

[2] S. Lecompte, H. Huisseune, M. van den Broek, B. Vanslambrouck, M. D. Paepe, Review of organic rankine cycle (ORC) architectures for waste heat recovery, Renewable and Sustainable Energy Reviews 47 (2015) 448 – 461. doi:https://doi.org/10.1016/j.rser.2015.03.089.

[3] Y. Lu, A. P. Roskilly, X. Yu, The development and application of organic rankine cycle for vehicle waste heat recovery, in: Organic Rankine Cycle Technology for Heat Recovery, IntechOpen, 2018, p. 22.

[4] J. Zhang, K. Li, J. Xu, Recent developments of control strategies for organic rankine cycle (ORC) systems, Transactions of the Institute of Measurement and Control 41 (6) (2019) 1528–1539. doi:10.1177/0142331217753061.

[5] P. Tona, J. Peralez, Control of organic rankine cycle systems on board heavy-duty vehicles: a survey, IFAC-PapersOnLine 48 (15) (2015) 419 – 426, 4th IFAC Workshop on Engine and Powertrain Control, Simulation and Modeling E-COSM 2015. doi:https://doi.org/10.1016/j.ifacol.2015.10.060.

[6] J. Peralez, P. Tona, A. Sciarretta, P. Dufour, M. Nadri, Towards model-based control of a steam rankine process for engine waste heat recovery, in: 2012 IEEE Vehicle Power and Propulsion Conference, IEEE, 2012, pp. 289–294.

[7] V. Grelet, P. Dufour, M. Nadri, V. Lemort, T. Reiche, Explicit multi-model predictive control of a waste heat rankine based system for heavy duty trucks, in: 54th IEEE Conference on Decision and Control (CDC), IEEE, 2015, pp. 179–184. doi:10.1109/CDC.2015.7402105.

[8] E. W. Lemmon, M. L. Huber, M. O. McLinden, Nist reference fluid thermodynamic and transport properties–refprop, NIST standard reference database 23 (2002) v7.

[9] M. W. Braun, D. E. Rivera, A. Stenman, A 'Model-on-Demand' identification methodology for non-linear process systems, International Journal of Control 74 (18) (2001) 1708–1717. doi:10.1080/00207170110089734.

[10] J. Peralez, Récupération d'énergie par cycle de Rankine à bord d'un véhicule: commande et gestion énergétique., PhD Thesis, Université Claude Bernard Lyon 1 (2015).

[11] J. Mohammadpour, C. W. Scherer (Eds.), Control of Linear Parameter Varying Systems with Applications, Springer, 2012. doi:10.1007/978-1-4614-1833-7.

[12] O. Sename, P. Gaspar, J. Bokor (Eds.), Robust Control and Linear Parameter Varying Approaches, Vol. 437, Springer, 2013. doi:10.1007/978-3-642-36110-4.

[13] B. P. Rasmussen, A. G. Alleyne, Dynamic modeling and advanced control of air conditioning and refrigeration systems, phdthesis, University of Illinois at Urbana-Champaign (2006).

[14] J. Zhang, M. Lin, F. Fang, J. Xu, K. Li, Gain scheduling control of waste heat energy conversion systems based on an LPV (linear parameter varying) model 107 (2016) 773–783. doi:10.1016/j.energy.2016.04.064.

[15] R. Tóth, Modeling and Identification of Linear Parameter-Varying Systems, Vol. 403 of Lecture Notes in Control and Information Sciences, Springer Berlin Heidelberg, 2010. doi:10.1007/978-3-642-13812-6.

[16] B. Bamieh, L. Giarré, Identification of linear parameter varying models 12 (9) (2002) 841–853. doi:10.1002/rnc.706.

[17] P. Apkarian, P. Gahinet, G. Becker, Self-scheduled h_∞ control of linear parameter-varying systems: a design example 31 (9) (1995) 1251–1261. doi:10.1016/0005-1098(95)00038-X.

[18] C. Scherer, P. Gahinet, M. Chilali, Multiobjective output-feedback control via LMI optimization 42 (7) (1997) 896–911.

[19] P. Tona, J. Peralez, Control of Organic Rankine Cycle Systems on board Heavy-Duty Vehicles: a Survey, IFAC-PapersOnLine 48 (15) (2015) 419–426. doi:10.1016/j.ifacol.2015.10.060.